Field-programmable acoustic array for patterning micro-objects

Cite as: Appl. Phys. Lett. 116, 151901 (2020); https://doi.org/10.1063/5.0003147 Submitted: 31 January 2020 . Accepted: 26 March 2020 . Published Online: 13 April 2020

Kuan-Wen Tung, and Pei-Yu Chiou 🕛



COLLECTIONS



This paper was selected as an Editor's Pick







ARTICLES YOU MAY BE INTERESTED IN

High mobility and high thermoelectric power factor in epitaxial ScN thin films deposited with plasma-assisted molecular beam epitaxy

Applied Physics Letters 116, 152103 (2020); https://doi.org/10.1063/5.0004761

Molecular beam epitaxy and characterization of wurtzite Sc_xAl_{1-x}N

Applied Physics Letters 116, 151903 (2020); https://doi.org/10.1063/5.0002445

Demonstration and aging test of a radiation resistant strontium-90 betavoltaic mechanism Applied Physics Letters 116, 153901 (2020); https://doi.org/10.1063/1.5140780

Lock-in Amplifiers up to 600 MHz







Cite as: Appl. Phys. Lett. **116**, 151901 (2020); doi: 10.1063/5.0003147 Submitted: 31 January 2020 · Accepted: 26 March 2020 · Published Online: 13 April 2020







Kuan-Wen Tung¹ and Pei-Yu Chiou^{1,2,a)} (D

AFFILIATIONS

- ¹Department of Mechanical and Aerospace Engineering, University of California at Los Angeles, 420 Westwood Plaza, Los Angeles, California 90095, USA
- ²Department of Bioengineering, University of California at Los Angeles, 410 Westwood Plaza, Los Angeles, California 90095, USA
- ^{a)}Author to whom correspondence should be addressed: pychiou@g.ucla.edu. Tel.: (310) 825-8620

ABSTRACT

A field-programmable acoustic platform is introduced to enable re-configurable patterning of micro-objects into complex and non-periodic shapes with sub-wavelength resolution. Conventional acoustic methodologies are difficult in realizing versatile adjustments of potential energy profiles due to the constraint of the device structure. To tackle such a challenge, we present a digitally programmable, near-field acoustic platform that permits the generation of versatile potential profiles. This platform uses an array of aqueous-medium filled cavities that can be selectively vaporized by a laser beam to pattern the acoustic wavefront of a plane wave to shape acoustic potential profiles. We have demonstrated a field-programmable acoustic platform with a digital pixel resolution of 40 μ m pitch. With a 17 mW, 532 nm laser, an air cavity can be generated at a rate of 1 cavity/s.

Published under license by AIP Publishing. https://doi.org/10.1063/5.0003147

Acoustics has long been applied for manipulating biological objects for its superior biocompatibility as compared to other physical mechanisms.^{1–8} Recent advancements in this field have also led to the increase in the degree-of-freedom (DOF) of manipulation. Starting with single-cell patterning, acoustics has evolved such that the size of the acoustic potential well can be optimized to allow only a single cell to occupy. The impact is profound for many biomedical applications,^{9–13} especially for large batch single-cell analysis. ¹⁴ Furthermore, three-dimensional phase-shifting based acoustic manipulation technology allows picking up and releasing single cells one by one. ¹⁵

In general, acoustic manipulation can be classified into surface acoustic wave (SAW)^{14–27} and bulk acoustic wave (BAW)^{28–31} approaches. Both approaches rely on an acoustic radiation force (ARF) generated in non-uniform acoustic potential fields to manipulate particles. For particles of size less than the applied wavelength ($D \ll \lambda$), the ARF on a particle and the potential field can be described by the following equations:³²

$$ARF = -\nabla U^{rad},\tag{1}$$

$$U^{rad} = \frac{4\pi}{3} a^3 \left\{ \left[1 - \frac{\kappa_p}{\kappa_0} \right] \frac{1}{2} \kappa_o \langle p^2 \rangle - \left[\frac{2 \left(\frac{\rho_p}{\rho_0} - 1 \right)}{2 \frac{\rho_p}{\rho_0} + 1} \right] \frac{3}{4} \rho_o \langle v^2 \rangle \right\}, (2)$$

where a is the radius of the particle and p and v represent the firstorder acoustic pressure and velocity at the particle's position. The material compressibility κ and density ρ are denoted by "p" and "o" for the particle and the surrounding medium, respectively. In order to generate non-uniform potential fields, BAW and SAW devices typically rely on forming acoustic standing waves created by resonant cavities and interdigitated transducers (IDTs), respectively. For BAWs, one drawback is that the potential profile is predetermined by the structural design of devices, which fundamentally prevents the patterning profile to be versatile and re-configurable. For SAW devices, although the potential profile can be adjusted by changing the phases and frequencies of the electrical signals applied to the IDTs,¹ complex patterning profiles are only obtained for single-particle manipulation, whereas the profiles for multi-particle manipulation are simple and periodic. Additionally, creating non-uniform fields using standing waves limits the patterning resolution to half of the acoustic wavelength. Another approach using holographic acoustic tweezers, based on an array of sound emitters, has also been demonstrated. Even though the approach is able to generate complex potential profiles, the spatial resolution remains low.³⁴

Recently, a type of acoustic manipulation platform called compliant membrane acoustic patterning (CMAP) was introduced to enable sub-wavelength resolution patterning of micro-particles into complex and non-periodic shapes. The potential profiles formed using

CMAP, however, are dependent on the predefined air cavity structures. Creating a new potential profile would require a different physical cavity structure to be fabricated.

Here, we present a field-programmable acoustic array (FPAA) in which the acoustic potential field can be optically re-configured for patterning micro-particles into complex non-periodic shapes with sub-wavelength resolution. The platform, Fig. 1, uses a combined PZT (lead zirconate titanate from APC International Ltd. and of material type 841) and a 1 μ m thick hydrogenated amorphous silicon (a-Si:H) film coated glass substrate to house an air-embedded, viscoelastic polydimethylsiloxane (PDMS) structure. The PDMS structure, molded into an array of squared air cavities, is a universal platform that can be re-configured to provide different potential profiles for patterns as demonstrated in the subsequent experiments (see Fig. 1S in the supplementary material for the detailed fabrication process). The experimental procedures include in four steps. Initially, Dulbecco's modified essential medium (DMEM) from corning is dispensed over the surface of the fabricated PDMS structure, Fig. 1(a). Through a vacuuming process, Fig. 1(b), DMEM goes through the porous PDMS membrane, 37,38 converting the air-embedded structure into a fluidembedded structure. DMEM, containing mostly water, is used for its similar acoustic impedance to that of PDMS.³⁹ We have also experimentally observed that DMEM goes through the PDMS membrane easier than does de-ionized (DI) water, possibly due to surface tension related properties. Any excessive DMEM on the PDMS surface is removed thereafter. Next, by focusing a continuous wave (CW), 532nm wavelength, 17 mW laser onto the wavelength 532nm onto the a-Si:H layer, the DMEM within the selected cavity is heated and

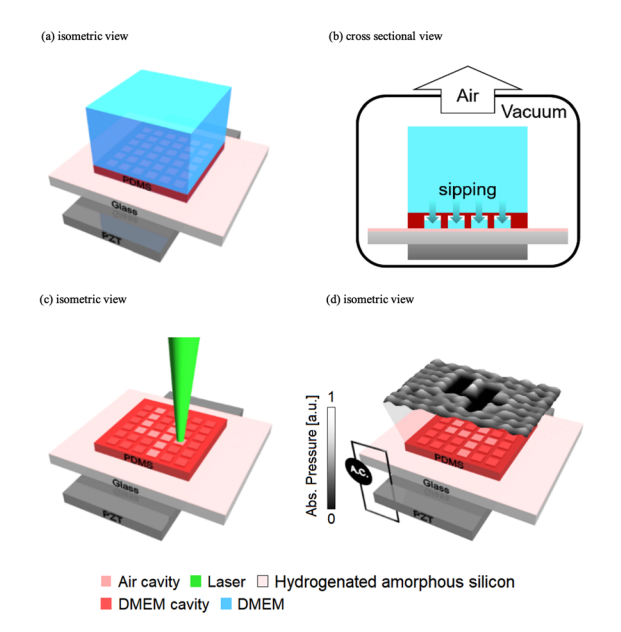


FIG. 1. Device schematics of the FPAA. The operation consists of four steps. First, DMEM is dispensed over the polydimethylsiloxane (PDMS) structure (a). Second, vacuuming is performed to fill the air cavities with the fluid by going through the PDMS membrane (b). Third, a focused laser beam is scanned through the fluid-embedded structure to selectively revert the fluid cavities to air cavities (c). Finally, PZT is activated, which enables acoustic waves to pass through the transformed structure to form the patterned, acoustic potential profile (d).

vaporized, Fig. 1(c). As a result, a series of cavities can be converted by scanning the laser beam across the PDMS structure, forming a desired shape like the numerical letter "4." The vapor created can diffuse through the PDMS membrane into the above air ambience. Subsequent activation of the PZT generates an acoustic potential profile based on the laser-created air cavity pattern, Fig. 1(d). For details of the experimental setup, refer to Fig. 2S in the supplementary material. In order to form micro-particle patterns, a fluid sample containing micro-particles is dispensed over the transformed structure. A 1 cm thick PDMS layer is then used to sandwich the fluid sample in between. This PDMS layer is used for absorbing acoustic traveling waves to prevent reflection from the ambience, which may result in interference patterns in the fluid. Upon turning on the PZT power, the micro-particles in the fluid will align with respect to the patterned potential profiles. Reprogramming the platform can be done by reapplying the vacuuming step introduced in Fig. 1(b), which can refill all

Spacing between these air cavities is a crucial parameter. Too large a spacing prevents the acoustic potential profiles of neighboring cavities from merging into one. To investigate this effect, we simulated the acoustic-structure interaction using a finite element model (COMSOL Multiphysics 5.3) and followed the simulation technique introduced in the previous work.³⁶ An array of 30 μ m wide air cavities is simulated with varying spacings at a sinusoid excitation frequency of 3 MHz. The 30 μ m cavity width is chosen to ensure sufficient attenuation of waves propagating into the PDMS membrane in order to avoid distortion to the potential profile generated. Based on the previous work, the attenuation length from the bulk into the membrane is estimated to be 10 μ m for a 2 μ m thick soft PDMS membrane.³⁶ The results, Fig. 2, show noticeable differences in the normalized acoustic radiation potential profiles, calculated based on $10 \,\mu m$ polystyrene beads in DI water, for cavity spacings between 60 μ m and 10 μ m. The potential profile for the 60 μ m spacing case, Fig. 2(a), fluctuates with energy dips at the edges of each air cavity, where the beads will tend to accumulate in the early stage of patterning. Such a characteristic is attributed to the dominance of the velocity term in Eq. (2) due to the large membrane vibration near the membrane edges. 36 For the 10 μ m spacing case, Fig. 2(b), the potential profile is smooth and flat with

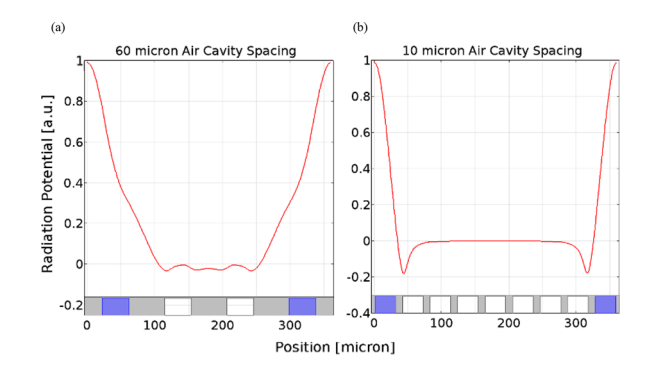


FIG. 2. Simulated, normalized acoustic potential profiles for an array of air cavities with a width of 30 μ m and varying cavity spacings. At a spacing of 60 μ m (a), the profile that is 5 μ m above the PDMS structure fluctuates with energy dips at the cavity edges. At a spacing of 10 μ m (b), the profile becomes nearly flat across, with dips only at the edges of the outer most cavities. Cavities in white represent air, and cavities in blue represent fluid.

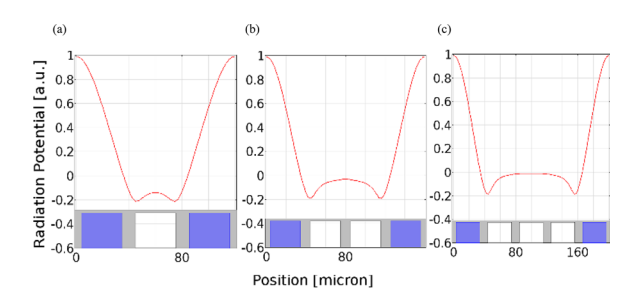


FIG. 3. Simulated, normalized acoustic potential profiles for an array of varying numbers of air cavities with a width of 30 μ m and a fixed cavity spacing of 10 μ m. The results for a single air cavity (a), two air cavities (b), and three air cavities (c) show similar profile shapes that have the lowest energy dips at the edges of the outer most cavities. Cavities in white represent air, and cavities in blue represent fluid

dips only at the outer most air cavities. This effect allows the potential profiles created by discrete air cavities to be merged into one profile of desired shape. To verify this coalescent effect, we also examined the impact of changing the number of nearby air cavities. The results,

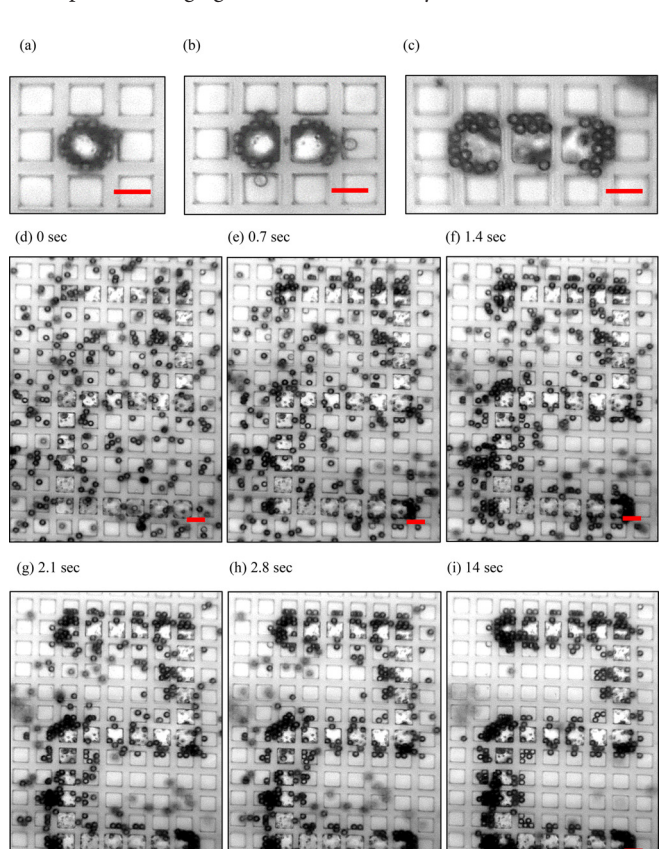


FIG. 4. Experimental demonstrations showing patterning of 10 μ m polystyrene beads using FPAA. Experimental results for a single air cavity (a), two air cavities (b), and three air cavities (c) conform to the simulation results in Figs. 3(a)–3(c). Shown in (d)–(i) is a patterning process for numerical letter "2." Scale bar, 30 μ m. Multimedia view: https://doi.org/10.1063/5.0003147.1

Fig. 3, show that the coalescent effect holds, and varying the number of cavities essentially only changes the size of the merged acoustic potential well. Note that at our operating frequency of 3 MHz, the wavelength in water is $\sim\!500\,\mu\text{m}$, which is substantially larger than the cavities' width and spacing. This demonstrates that the FPAA allows the formation of acoustic potential profiles with sub-wavelength resolution.

To verify the simulation results, we carried out experiments by following the setup shown in Fig. 2S in the supplementary material. With a sample of 10 μm polystyrene beads in DMEM dispensed over a patterned FPAA platform, the beads' profiles obtained match those of the simulations. Figures 4(a)–4(c) experimentally illustrate the coalescent effect of squared air cavities of width 30 μm spaced 10 μm apart. In Fig. 4(a), beads are distributed around the edges of a single air cavity where the lowest acoustic potential resides. With two and three air cavities, Figs. 4(b) and 4(c), beads are distributed only at the outer most edges of the cavities. In between the cavities, beads do not occupy; such a phenomenon confirms the coalescent effect of potential profiles created by closely spaced air cavities.

To demonstrate the patterning capability of the FPAA platform, we patterned micro-particles into complex and non-periodic shapes. Shown in Figs. 4(d)-4(i) (Multimedia view) are snapshots of the process of $10 \,\mu m$ polystyrene beads forming into letter 2. In Fig. 4(i), a majority of micro-particles trapped along the outer most edges of air cavities match with what is predicted by the simulation. Additional patterning examples are demonstrated in Fig. 3S in the supplementary material.

In conclusion, a field-programmable acoustic array (FPAA) has been demonstrated. Such a platform is capable of re-configurable patterning of micro-objects into complex and non-periodic shapes at a resolution of 40 μ m under the excitation of 3 MHz signals. Higher resolution is possible through increasing the acoustic frequencies; yet, effects such as increased energy absorption may need to be properly managed. In FPAA, programmable patterning is realized by applying laser heating to selectively vaporize fluid in a two-dimensional PDMS micro-cavity array. With the spacing between cavities reduced to $10 \,\mu \text{m}$, acoustic potential profiles generated by neighboring cavities can be merged to form an integrated complex potential profile. Reprogramming is realized by simply reapplying a vacuuming step to refill the air cavities with fluid that resets the platform. With the described features, FPAA is versatile for applications in microfluidics such as biological micro-particle patterning, sorting, tissue engineering, and advanced manufacturing for 3D printing.

See the supplementary material for detailed information on fabrication of the FPAA cavity structure, experimental setup, and additional examples of complex patterning (supplementary material figures); patterning process for numerical letter 2 and laser-induced vaporization of DMEM (supplementary material multimedia views); and supplementary material reference.

This work was supported by No. NSF ECCS 1711507. We also thank the Nanoelectronics Research Facility at the University of California at Los Angeles.

REFERENCES

¹W. Hu, Q. Fan, and A. T. Ohta, Lab Chip 13, 2285 (2013).

- ²M.-C. Zhong, X.-B. Wei, J.-H. Zhou, Z.-Q. Wang, and Y.-M. Li, Nat. Commun. 4, 1768 (2013).
- ³A. Ashkin, J. M. Dziedzic, and T. Yamane, Nature **330**, 769 (1987).
- ⁴H. Zhang and K.-K. Liu, J. R. Soc. Interface 5, 671 (2008).
- ⁵B. Lim, V. Reddy, X. Hu, K. Kim, M. Jadhav, R. Abedini-Nassab, Y.-W. Noh, Y. T. Lim, B. B. Yellen, and C. Kim, Nat. Commun. 5, 3846 (2014).
- ⁶C.-T. Ho, R.-Z. Lin, R.-J. Chen, C.-K. Chin, S.-E. Gong, H.-Y. Chang, H.-L. Peng, L. Hsu, T.-R. Yew, S.-F. Chang, and C.-H. Liu, Lab Chip 13, 3578 (2013)
- ⁷M.-Y. Chiang, Y.-W. Hsu, H.-Y. Hsieh, S.-Y. Chen, and S.-K. Fan, Sci. Adv. 2, e1600964 (2016).
- ⁸I.-F. Cheng, H.-C. Chang, D. Hou, and H.-C. Chang, Biomicrofluidics 1, 021503 (2007).
- ⁹J. Nilsson, M. Evander, B. Hammarström, and T. Laurell, Anal. Chim. Acta **649**, 141 (2009).
- ¹⁰L. Kang, Drug Discovery Today **13**, 1 (2008).
- 11 L. Gervais, N. de Rooij, and E. Delamarche, Adv. Mater. 23, H151 (2011).
- ¹²D. Taller, K. Richards, Z. Slouka, S. Senapati, R. Hill, D. B. Go, and H.-C. Chang, Lab Chip 15, 1656 (2015).
- ¹³C. M. Puleo, H.-C. Yeh, and T.-H. Wang, Tissue Eng. 13, 2839 (2007).
- ¹⁴D. J. Collins, B. Morahan, J. Garcia-Bustos, C. Doerig, M. Plebanski, and A. Neild, Nat. Commun. 6, 8686 (2015).
- ¹⁵F. Guo, Z. Mao, Y. Chen, Z. Xie, J. P. Lata, P. Li, L. Ren, J. Liu, J. Yang, M. Dao, S. Suresh, and T. J. Huang, Proc. Natl. Acad. Sci. 113, 1522 (2016).
- ¹⁶X. Ding, S.-C. S. Lin, B. Kiraly, H. Yue, S. Li, I.-K. Chiang, J. Shi, S. J. Benkovic, and T. J. Huang, Proc. Natl. Acad. Sci. 109, 11105 (2012).
- ¹⁷A. K. Tay, M. Dhar, I. Pushkarsky, and D. D. Carlo, Lab Chip **15**, 2533 (2015).
- ¹⁸G. Destgeer and H. J. Sung, Lab Chip **15**, 2722 (2015).
- ¹⁹S.-C. Steven Lin, X. Mao, and T. J. Huang, Lab Chip **12**, 2766 (2012).

- ²⁰L. Y. Yeo and J. R. Friend, Biomicrofluidics 3, 012002 (2009).
- ²¹Y. Chen, X. Ding, S.-C. Steven Lin, S. Yang, P.-H. Huang, N. Nama, Y. Zhao, A. A. Nawaz, F. Guo, W. Wang, Y. Gu, T. E. Mallouk, and T. J. Huang, ACS Nano 7, 3306 (2013).
- 22X. Ding, J. Shi, S.-C. Steven Lin, S. Yazdi, B. Kiraly, and T. Jun Huang, Lab Chip 12, 2491 (2012).
- ²³Y. Bian, F. Guo, S. Yang, Z. Mao, H. Bachman, S.-Y. Tang, L. Ren, B. Zhang, J. Gong, X. Guo, and T. J. Huang, Microfluid. Nanofluid. 21, 132 (2017).
- ²⁴A. R. Rezk, J. K. Tan, and L. Y. Yeo, Adv. Mater. **28**, 1970 (2016).
- 25B. Kang, J. Shin, H.-J. Park, C. Rhyou, D. Kang, S.-J. Lee, Y. Yoon, S.-W. Cho, and H. Lee, Nat. Commun. 9, 5402 (2018).
- ²⁶W. Connacher, N. Zhang, A. Huang, J. Mei, S. Zhang, T. Gopesh, and J. Friend, Lab Chip 18, 1952 (2018).
- ²⁷M. Alvarez, J. R. Friend, and L. Y. Yeo, Langmuir 24, 10629 (2008).
- ²⁸B. Raeymaekers, C. Pantea, and D. N. Sinha, J. Appl. Phys. **109**, 014317 (2011).
- ²⁹I. Leibacher, P. Reichert, and J. Dual, Lab Chip **15**, 2896 (2015).
- ³⁰B. Hammarström, T. Laurell, and J. Nilsson, Lab Chip **12**, 4296 (2012).
- ³¹A. Castro and M. Hoyos, Ultrasonics **66**, 166 (2016).
- ³²H. Bruus, Lab Chip **12**, 1014 (2012).
- ⁵³Z. Tian, S. Yang, P.-H. Huang, Z. Wang, P. Zhang, Y. Gu, H. Bachman, C. Chen, M. Wu, Y. Xie, and T. J. Huang, Sci. Adv. 5, eaau6062 (2019).
- 34A. Marzo and B. W. Drinkwater, Proc. Natl. Acad. Sci. 116, 84 (2019).
- ³⁵K. Melde, A. G. Mark, T. Qiu, and P. Fischer, Nature **537**, 518 (2016).
- ³⁶K.-W. Tung, P.-S. Chung, C. Wu, T. Man, S. Tiwari, B. Wu, Y.-F. Chou, F. Yang, and P.-Y. Chiou, Lab Chip 19, 3714 (2019).
- ³⁷E. Verneuil, A. Buguin, and P. Silberzan, Europhys. Lett. **68**, 412 (2004).
- ³⁸G. C. Randall and P. S. Doyle, Proc. Natl. Acad. Sci. **102**, 10813 (2005).
- ³⁹F. Sabri, M. E. Sebelik, R. Meacham, J. D. Boughter, M. J. Challis, and N. Leventis, PLoS One 8, e66348 (2013).